New anionic states of the lithium trimer

Maciej Gutowski[a] and Jack Simons
Chemistry Department, University of Utah, Salt Lake City, Utah 84112

(Received 5 January 1994; accepted 25 May 1994)

Anionic states of Li_3 were studied theoretically using a full-valence complete active space (CAS) self-consistent field (SCF) approach to explore their potential energy surfaces followed by quadratic configuration interaction with single, double, and approximate triple excitations calculations to more accurately determine relative energies and electron detachment energies. In addition to the known $^1\Sigma_g^+$ state, one triplet ($^3A_2'$) and two quintet ($^5A_1''$ and $^5A_2'$) states were found to be relatively low lying and electronically and geometrically stable in D_{3h} geometries. All of these states remain electronically stable in C_{2v} and $D_{\infty h}$ geometries. Hence, they are amenable to photoelectron spectroscopy detection. Preliminary CAS SCF results for the valence isoelectronic Na_3^- are also reported.

I. INTRODUCTION

Alkali metal trimers may be considered as prototype clusters involving three monovalent *s*-orbital radicals. An excellent review on the neutral, cationic, and anionic alkali metal clusters has recently been published by Bonacic-Koutecky *et al.*[1] Our interests in double-Rydberg anions[2] as well as in chemical bonds between Rydberg radicals[3] led us to this study on anionic states of the alkali metal trimers.

We recently studied several low lying doublet and quartet states of the neutral lithium trimer.[4] In addition to the well-known pseudorotating ground state we considered excited electronic states which were recently explored using the two photon ionization technique.[5,6] Our results suggested a new assignment of the experimental peaks.

In this study we explore *anionic* states of the lithium and sodium trimers. Photodetachment spectra of the alkali metal trimers other than Li_3^- were reported by Bowen's group a few years ago,[7] whereas the spectrum of Li_3^- has only recently been recorded.[8] The lithium clusters are difficult for experimental studies due to the high temperatures necessary to heat the metal and the corrosive properties of lithium.[9]

Photoelectron spectra of all M_3^- species (M=alkali metal atom) are dominated by two distinct and well-separated peaks. These peaks are assigned to transitions beginning in the linear $^1\Sigma_g^+(\sigma_g^2\sigma_u^2)$ state of M_3^-, with the resulting neutral species formed either in the ground $^2\Sigma_u^+(\sigma_g^2\sigma_u^1)$ or in the excited $^2\Sigma_g^+(\sigma_g^1\sigma_u^2)$ state.

For the ground $^2\Sigma_u^+$ state, the vertical detachment energy (VDE) is 1.309 ± 0.005 and 1.158 ± 0.010 eV, for Li_3^- and Na_3^-, respectively.[7,8] Upon bending, the $^2\Sigma_u^+$ state correlates with the lowest $^2B_2$ state (a local minimum on the pseudorotating ground state surface of the neutral). In earlier work, we indeed verified that linear Li_3 in the $^2\Sigma_u^+$ state is unstable with respect to the bending motion.[4] Hence, for the $^2\Sigma_u^+ + e \leftarrow {}^1\Sigma_g^+$ transition, one can expect a difference between the VDE and adiabatic electron affinity (EA_a) equal roughly to the linearization energy of the ground state of M_3.

For the second $^2\Sigma_g^+ + e \leftarrow {}^1\Sigma_g^+$ transition, the experimental VDE is 2.003 ± 0.005 and 1.813 ± 0.010 eV, for Li_3^- and Na_3^-, respectively.[7,8] Our earlier work shows that the $^2\Sigma_g^+$ state is stable with respect to bending motion,[4] hence the discrepancy between the VDE and EA_a is expected to be small for this transition.

Past theoretical studies on the anionic alkali metal trimers concentrated on the linear structure. Boustani and Koutecky found the $^1\Sigma_g^+$ state of Li_3^- to be geometrically stable at the self-consistent field (SCF) level of theory, which was consistent with the electrostatic repulsion argument.[10] Electron detachment energies from the linear structures of Li_3^- and Na_3^- were studied by Ortiz using electron propagator theory[11] and by Bonacic-Koutecky *et al.* using the configuration interaction (CI) approach.[12] These theoretical results match the experimental data with an accuracy of 0.07 eV.

In the present work, we start from the monomers and dimers of the alkali metals to calibrate the accuracy of our calculations. The anions of M_2 are of particular interest. The photoelectron spectrum of Na_2^- was reported in Ref. 7, whereas that of Li_2^- has only recently been recorded.[13] Three observed electronic bands are assigned to transitions from the $X\,^2\Sigma_u^+(\sigma_g^2\sigma_u)$ bound state to $X\,^1\Sigma_g^+(\sigma_g^2)$, $a\,^3\Sigma_u^+(\sigma_g\sigma_u)$, and $A\,^1\Sigma_u^+(\sigma_g\sigma_u)$ states of M_2. A Franck–Condon analysis of the lowest electron binding energy band allows one to determine spectroscopic constants of $^7Li_2^-$.[13]

Our monomer and dimer calibration studies are followed by a thorough exploration of the singlet, triplet, and quintet states of Li_3^- for D_{3h}, C_{2v}, and $D_{\infty h}$ geometries. To the best of our knowledge, the only other study in which a nonsinglet anionic state was considered is that of Boustani and Koutecky.[10] They concluded that a linear stationary point of the lowest triplet state is not a minimum at the SCF level of theory, so they subsequently focused their attention on the linear singlet state.

In our study, the singlet, triplet, and quintet surfaces are explored at the full-valence complete active space (CAS) SCF level of theory. More accurate relative energies and electron detachment energies are determined at the quadratic configuration interaction (QCI) level.[14]

Presentation of our detailed results for Li_3^- is followed

[a]Present address: IBM Research Division, Almaden Research Center, 650 Harry Road, San Jose, CA 95120-6099.

 0021-9606/94/101(6)/4867/11/$6.00

by our preliminary results for Na_3^-. Guided by the lithium trimer results, we located stationary points on the full-valence CAS SCF potential energy surfaces of the neutral and anionic Na_3, after which VDEs and EA_a's were determined at the same level of theory.

In addition to the lowest energy $^1\Sigma_g^+$ anionic state, we have found that a triangular $^3A_2'(a_1'^2e'^2)$ state is electronically and geometrically stable for both alkali metal trimer anions. The electronic stability is preserved along a path from the D_{3h} minimum through C_{2v} structures to a linear local minimum (producing a $^3\Sigma_u^+$ state).

Another two previously unexplored triangular anionic states of $^5A_1''(a_1'e'^2a_2'')$ and $^5A_2'(a_1'e'^2a_1')$ symmetry were also found to be geometrically stable. They are also electronically stable with respect to the lowest neutral *quartet* $^4A_2'(a_1'e'^2)$ state. Hence, they are genuine bound states in the nonrelativistic approximation since they cannot decay to lower lying (e.g., $X\ ^1\Sigma_g^+$) anion states due to spin and orbital occupancy restrictions. The electronic stability of these quintet states is preserved along a C_{2v} path which connects the D_{3h} and $D_{\infty h}$ geometry. At linear geometry, these two quintet states correlate to a $^5\Pi_g(\sigma_g^1\sigma_u^1\sigma_g^1\pi_u)$ state. The $^5A_1''$ state preserves a positive curvature along the antisymmetric stretching mode in C_{2v} geometries, but the $^5A_2'$ state ($^5B_2$ in C_{2v}) is coupled through second-order Jahn–Teller interaction with another quintet $^5A_1$ state to yield negative curvature along the b_2 asymmetric stretch mode.

In Sec. II we discuss computational aspects of this study; Sec. III covers the anionic monomers and dimers, and in Sec. IV our results for the singlet, triplet, and quintet states of Li_3^- and Na_3^- are presented. In Sec. V we summarize.

II. COMPUTATIONAL ASPECTS

The one-electron atomic basis sets for the lithium atom are detailed in Table I. The smaller one, labeled D, consists of Dunning's double-zeta $(9s5p/3s2p)$ one-electron basis set[15] supplemented with diffuse s and p functions with the same exponent 0.0074[16] and one d function with the exponent 0.2.[17] The larger basis set, labeled T, consists of Dunning's triple-zeta $(12s6p/4s3p)$ set supplemented with the diffuse s and p functions[16] and two d functions with exponents 0.3 and 0.15. For the sodium atom we used the McLean and Chandler $(12s9p/6s5p)$ set[18] supplemented with diffuse s and p functions with the same exponent 0.0076[19] and one d polarization function with the exponent 0.175.[20]

The ground and excited potential energy surfaces for the neutral and anionic M_3 were studied at the CAS SCF level of theory, with the D basis set for Li_3. The molecular orbitals derived from atomic core orbitals ($1s$ for Li, $1s$, $2s$, and $2p$ for Na) were doubly occupied in every configuration state function (CSF). The resulting neglect of the core–core and core–valence correlation effects yields results we label *frozen core approximation* in subsequent discussion. These correlation effects are negligible for lithium and small for the sodium clusters due to low polarizability of the M^+ cores.[21] The remaining three (neutral) or four (anion) electrons were distributed in all possible ways among the molecular orbitals derived from the atomic valence ns and np orbitals. This choice of the active space led to 572 and 220 SCFs for the doublet and quartet states of M_3. For the anion, the number of SCFs is 1716, 2145, and 495 for singlet, triplet, and quintet states, respectively. The CAS SCF calculation for the dimer and the atomic species were performed with the analogous active spaces (i.e., frozen core approximation plus all valence orbitals in the active space).

The CAS SCF calculations were performed with the Utah MESS-KIT modular electronic structure codes[22] which generate the analytical second geometrical derivatives. Geometrical minima and transition states on the three-

TABLE I. The Gaussian one-electron basis sets used for the lithium atom (Refs. 15–17).

Symmetry	Exponent	Contraction coefficients	
		D basis set	
s	1469.0	0.000 766	−0.000 120
	220.5	0.005 892	−0.000 923
	50.26	0.029 671	−0.004 689
	14.24	0.109 180	−0.017 682
	4.581	0.282 789	−0.048 902
	1.580	0.453 123	−0.096 009
	0.564	0.274 774	−0.136 380
	0.073 45	0.009 751	0.575 102
	0.028 05	−0.003 18	0.517 661
s	0.028 05	1.0	
s	0.007 4	1.0	
p	3.250 0	0.008 691	
	0.647 4	0.047 819	
	0.168 9	0.210 615	
	0.055 61	0.528 695	
	0.020 47	0.381 375	
p	0.020 47	1.0	
p	0.007 40	1.0	
d	0.2	1.0	
		T basis set	
s	6601.0	0.000 117	−0.000 018
	989.7	0.000 911	−0.000 142
	225.7	0.004 728	−0.000 741
	64.29	0.019 197	−0.003 020
	21.18	0.063 047	−0.010 123
	7.724	0.163 208	−0.027 094
	3.003	0.314 827	−0.057 359
	1.212	0.393 936	−0.093 895
	0.493	0.196 918	−0.121 091
	0.095 15	0.009 997	0.276 608
	0.047 91	−0.005 402	0.549 548
	0.022 20	0.001 704	0.277 385
s	0.047 91	1.0	
s	0.022 20	1.0	
s	0.007 40	1.0	
p	5.928	0.003 668	
	1.295	0.020 596	
	0.349 3	0.083 282	
	0.115 4	0.279 201	
	0.044 01	0.514 145	
	0.017 84	0.278 900	
p	0.044 01	1.0	
p	0.017 84	1.0	
p	0.007 4	1.0	
d	0.3	1.0	
d	0.15	1.0	

dimensional potential energy surfaces have been determined using our automated surface walking algorithm.[23] In cases where a small energy gap between electronic states of the same symmetry occurs, the CAS SCF wave-function optimization for the higher state was performed in the state-averaged (SA) fashion,[24] in which case only first analytical derivatives were available.[25]

The full-valence CAS SCF method is sufficient to deliver detailed information about the potential energy surfaces. In particular it can deal with multiconfigurational problems. For $^1B_2$ anionic state, however, the nature of a stationary point (minimum) determined at this CAS SCF level was counterintuitive. In particular, the curvature along the asymmetric stretching mode was questionable. In this dubious case, we also examined the results obtained using CAS active spaces smaller and larger than the full-valence space. These numerical tests strongly suggest that the $^1B_2$ stationary point is a transition state rather than a minimum.

Due to the small number of valence electrons and the full-valence active space, our CAS SCF electron detachment energies are quite accurate. For instance, the VDEs for Na_3^- are off by at most 0.08 eV, for the two experimentally known transitions. Even more accurate detachment energies were determined for Li_3^- at the quadratic configuration interaction level with single, double, and approximate triple excitations [QCISD(T)].[14] This method takes into account dynamical correlation effects and, due to its inherent size extensivity, it is well suited to deliver reliable electron detachment energies. Moreover, in our QCI calculations we removed the frozen core approximation so all core electrons were correlated. The QCISD(T) results were obtained with the GAUSSIAN 92 suite of codes[26] using both the D and T basis sets. The difference in the electron detachment energies did not exceed 0.04 eV, thus, to conserve space, only the T basis set results are presented in later discussion. We expect that the reported detachment energies may still be in error by ~0.02 eV primarily due to: (i) inaccuracy of the geometrical parameters, (ii) neglect of f-symmetry basis functions.

Finally, the oscillator strength for the $^5A_2' \leftarrow {}^5A_1''$ transition was calculated at the first-order configuration interaction (FOCI) level from the full-valence CAS reference space using the GAMESS package[27] and the D basis set.

III. ATOMS AND DIMERS

Our CAS SCF and QCI separation between the atomic ^2S and ^2P states of Li is 1.84 eV. It compares well with the experimental data of 1.85 eV.[28] For Na, however, the CAS SCF $^2S-{}^2P$ separation is too low by 0.13 eV in comparison with the experimental value of 2.10 eV.[28] This larger discrepancy for Na is caused primarily by core–valence correlation effects which are neglected in our frozen-core approximation.[12]

Our CAS SCF electron affinities for Li and Na are 0.52 and 0.47 eV, respectively, compared with the experimental data of 0.62 and 0.55 eV.[29] A full-CI calculation for the two outermost valence electrons, still with the frozen core approximation, leads to results of 0.59 and 0.54 eV. Finally, the QCI result for Li with the frozen-core approximation released is 0.61 eV.

TABLE II. Full valence CAS SCF spectroscopic parameters for different electronic states of M_2 and the ground $^2\Sigma_u^+$ state of M_2^- (M=Li,Na). R_e in a.u., ω_e in cm^{-1}, D_0 in eV. The QCI SD(T) values for D_0 are in parentheses.

Species	State	R_e	ω_e	D_0
Li_2	$X\ ^1\Sigma_g^+$	5.15	343	0.92 (1.02)
		5.05[a]	351[a]	1.05[a]
Li_2	$a\ ^3\Sigma_u^+$	8.18	52	0.02 (0.04)
		8.00[b]	61[b]	0.03[b]
Li_2	$b\ ^3\Pi_u$	5.01	335	1.31 (1.46)
		4.96[c]	342[c]	1.42[c]
Li_2	$A\ ^1\Sigma_u^+$	6.01	256	1.09
		5.93[c]	261[c]	1.14[c]
Li_2^-	$X\ ^2\Sigma_u^+$	5.85	230	0.75 (0.83)
		5.85[d]	232[d]	0.87[d]
Na_2	$X\ ^1\Sigma_g^+$	5.89	153	0.66
		5.82[a]	159[a]	0.72[a]
Na_2	$a\ ^3\Sigma_u^+$	10.29	20	0.02
		9.84[e]	25[f]	0.02[e]
Na_2	$b\ ^3\Pi_u$	6.07	145	1.00
		6.07[e]	155[f]	1.08[e]
Na_2	$A\ ^1\Sigma_u^+$	7.05	112	0.95
		6.88[a]	117[a]	1.00[a]
Na_2^-	$X\ ^2\Sigma_u^+$	6.85	98	0.55
				0.44[a]

[a]Reference 38.
[b]Reference 41.
[c]Reference 42.
[d]Reference 13.
[e]Reference 40.
[f]Reference 39.

These results demonstrate that our full-valence CAS SCF approach and the D orbital basis set are capable of delivering reliable $S-P$ energy separations between valence electronic states (accuracy ~0.15 eV) as well as meaningful electron affinities (low by ~0.1 eV). The inaccuracy of the CAS SCF VDEs is primarily caused by insufficient correlation between valence electrons. Refinement of the valence electronic states separations requires inclusion of core–valence and core–core correlation effects.

Our CAS SCF equilibrium internuclear distances, harmonic vibrational frequencies, and dissociation energies for the four lowest electronic states of Li_2 and Na_2 are reported in Table II. The agreement with other theoretical and experimental results is satisfactory. The discrepancies in equilibrium geometries do not exceed 0.1 a.u., with the exception of the weakly bound $a\ ^3\Sigma_u^+$ state where due to the shallow potential energy depth ($D_e \approx 0.02$ eV), a larger discrepancy (0.45 a.u.) is reported for Na_2. The harmonic vibrational frequencies match the experimental/theoretical results to within 10 cm^{-1} which is better than expected. The CAS SCF and QCI errors in D_0 values do not exceed 0.12 and 0.04 eV, respectively. For the $^1\Sigma_u^+$ excited state the QCI result was unreliable, probably due to the serious spin contamination at the UHF level. Only the CAS SCF results are reported for this state.

In Table II we also present CAS SCF spectroscopic parameters for Li_2^- and Na_2^-. The agreement with the available experimental results for Li_2^- (Ref. 13) is excellent for R_e and ω_e, but D_0 is off by 0.12 (CAS) and 0.04 eV (QCI).

In Table III we present VDEs and EA_a's relative to the

TABLE III. CAS SCF and QCI SD(T) vertical electron detachment energies (VDE) and adiabatic electron affinities (EA_a) in eV for the $X\ ^2\Sigma_u^+$ state of X_2^- (X=Li, Na). Experimental results in parentheses.

Transition	Method	VDE	EA_a
$Li_2(^1\Sigma_g^+)+e\leftarrow Li_2^-$	CAS	0.42	0.34
	QCI	0.515(0.52)[a]	0.414(0.44)[a]
$Li_2(^3\Sigma_u^+)+e\leftarrow Li_2^-$	CAS	1.37	1.26
	QCI	1.497	1.406
$Li_2(^3\Pi_u)+e\leftarrow Li_2^-$	CAS	1.90	1.79
	QCI	1.948	1.807
$Li_2(^1\Sigma_u^+)+e\leftarrow Li_2^-$	CAS	2.02	2.02
$Na_2(^1\Sigma_g^+)+e\leftarrow Na_2^-$	CAS	0.43(0.543)[b]	0.35(0.430)[b]
$Na_2(^3\Sigma_u^+)+e\leftarrow Na_2^-$	CAS	1.13	1.00
$Na_2(^3\Pi_u)+e\leftarrow Na_2^-$	CAS	2.04	1.98
$Na_2(^1\Sigma_u^+)+e\leftarrow Na_2^-$	CAS	2.04	2.03

[a]Reference 13.
[b]Reference 7.

bound $^2\Sigma_u^+$ ground state of the anion. For the lowest VDE of Li_2^-, the agreement between our theoretical (QCI) and the experimental value is within 0.01 eV. The difference between the VDE and EA_a is the smallest for the $Li_2(^1\Sigma_u^+)+e\leftarrow Li_2^-$ transition due to the similarity in equilibrium geometries of the neutral and the anion. The $Li_2(^3\Pi_u)+e\leftarrow Li_2^-$ transition was not (yet) observed experimentally,[13] probably due to its two-electron (i.e., shake up) nature. The CAS SCF results systematically underestimate the VDE by ~0.1 eV in comparison with the experimental results.

IV. TRIMERS

Anionic states of M_3^- have been explored in D_{3h}, C_{2v}, and $D_{\infty h}$ geometries. The dominant electronic configurations of the numerous low-energy anionic and neutral states can best be clarified using the molecular orbital correlation diagram for *nsnp* atoms shown in Fig. 1.

Several electronic states (e.g., $^1\Sigma_g^+$, $^3A_2'$, $^5A_1''$, $^5A_2'$) are electronically stable for a wide range of molecular geometries and are discussed in Sec. IV A. Many other states, such as $^5\Sigma_g^+$, $^5\Sigma_u^-$, $^3\Sigma_g^+$, $^3\Pi_g$, $^1A_1'$, $2\ ^5A_2$, are electronically stable only for a limited range of molecular geometries. Certain of these, such as the $2\ ^5A_2$ state are promising candidates for long-lived metastable states. Others, such as the $^5\Sigma_g^+$ state, cross the energy surface of the ground electronic state of the same multiplicity and thus have reduced lifetimes. All of these latter electronic states will be discussed in Sec. IV B.

The dominant electronic configurations, equilibrium geometries, harmonic vibrational frequencies, and relative energies are reported in Table IV for electronically stable (globally or locally) states of Li_3^-. Calculated values of the VDEs and EA_a's for various anion states are shown in Tables V and VI for Li_3^- and Na_3^-, respectively.

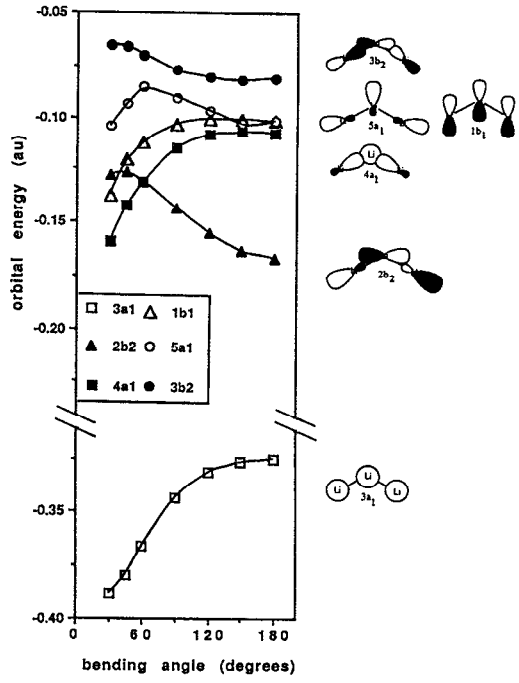

FIG. 1. Molecular orbital correlation diagram for the lithium trimer as a function of the bending angle θ which is equal to 60° and 180° for the D_{3h} and $D_{\infty h}$ structure, respectively. The SCF orbital energies were obtained for the closed-shell cation Li_3^+, with the $3a_1$ orbital doubly occupied.

A. Globally electronically stable states

1. D_{3h} geometries and the C_{2v} neighborhood

The lowest energy electronic configuration in D_{3h} geometry, $(2a_1'^2 2e'^2)$ produces the following electronic states: $1\ ^3A_2'$, $1\ ^1E'$, and $1\ ^1A_1'$. All of these states are electronically stable with respect to the neutral $^2E'(2a_1'^2 2e')$. In addition, two quintet Li_3^- anionic states were found to be electronically stable with respect to the lowest quartet neutral state $^4A_2'(2a_1'2e'^2)$. The latter are the $^5A_1''(2a_1'2e'^2 1a_2'')$ and $^5A_2'(2a_1'2e'^2 3a_1')$ states.

a. $^3A_2'$ *state.* This is the lowest energy anionic state in D_{3h} geometries. The CAS SCF equilibrium $M-M$ separations are 5.93 and 7.09 a.u. for Li_3^- and Na_3^-, respectively. The Li_3^- harmonic vibrational frequencies [187 (e') and 235 (a_1') cm^{-1}] indicate that this is a true minimum on the potential energy surface. For Li_3^+ and Na_3^+, our CAS SCF equilibrium $M-M$ distances are 5.76 and 6.67 a.u., respectively, somewhat shorter than the anionic equilibrium geometries.

For Li_3^-, the VDE corresponding to the transition $^2E' + e\leftarrow {}^3A_2'$ is 0.761 eV at the QCI level and 0.679 eV at the CAS SCF level. Interestingly, the neutral M_3 thus produced would be in the neighborhood of the $^2E'$ conical intersection. Hence this triplet anionic state offers the experimental opportunity to prepare M_3 neutral clusters with initial geometries otherwise unavailable.

Since the ground state of the M_3 neutral is subject to first-order Jahn–Teller (FOJT) distortion, the value of EA_a

TABLE IV. Dominant electronic configurations followed by the CI coefficients, geometries (distances in a.u., angles in degrees), CAS SCF harmonic frequencies (in cm^{-1}) and relative CAS SCF and QCI SD(T) energies (in eV) for stationary points on different potential energy surfaces of Li_3^-.

State	Dominant configuration	Geometry	Frequencies	ΔE_{CAS}	ΔE_{QCI}
$^1\Sigma_g^+$	$3\sigma_g^2 2\sigma_u^2$ (0.84)	$D_{\infty h}$ $R=5.757$	$106(\pi_u)$ $184(\sigma_g)$ $284(\sigma_u)$	0.0	0.0
$^1B_2$[a]	$3a_1^2 4a_1 2b_2$ (0.87)	C_{2v} $R=6.193$ $\angle=55.193$	$173(a_1\text{bend})$ $252(a_1)$ $658i(b_2)$	0.68	
$^3A_2'$	$2a_1'^2 2e'^2$ (0.88)	D_{3h} $R=5.926$	$187(e')$ $235(a_1')$	0.46	0.379
$^3\Sigma_u^+$	$3\sigma_g^2 2\sigma_u 4\sigma_g$ (0.84)	$D_{\infty h}$ $R=6.030$	$53(\pi_u)$ $153(\sigma_g)$ $178(\sigma_u)$	0.74	0.705
$^5A_1''$	$2a_1'2e'^2 1a_2''$ (0.96)	D_{3h} $R=5.802$	$187(e')$ $221(a_1')$	1.70	1.571
$^5A_2'$	$2a_1'2e'^2 3a_1'$ (0.97)	D_{3h} $R=6.311$	$130(e')$ $184(a_1')$	1.82	1.700
$^5\Pi_g$	$3\sigma_g 2\sigma_u 4\sigma_g 1\pi_u$	$D_{\infty h}$ $R=6.083$	$51(\pi_u)$ $135(\sigma_g)$ $204(\sigma_u)$	1.98	1.902
$^1A_1'$	$2a_1'^2 2e'^2$ (0.72)	D_{3h} $R=5.928$	$245(a_1')$ $301(e')$	1.08	
$^3\Sigma_g^+$	$3\sigma_g 2\sigma_u^2 4\sigma_g$ (0.63)+ $3\sigma_g^2 2\sigma_u^2 3\sigma_u$ (0.60)	$D_{\infty h}$ $R=6.038$	$86(\pi_u)$ $161(\sigma_g)$ $303(\sigma_u)$	1.02	0.954
$^3\Pi_g$	$3\sigma_g^2 2\sigma_u 1\pi_u$ (0.77)	$D_{\infty h}$ $R=5.529$	$68(\pi_u)\rightarrow{}^3A_2$ $75(\pi_u)\rightarrow{}^3B_2$ $184(\sigma_g)$ $293(\sigma_u)$	1.20	1.122
$^5\Sigma_g^+$	$3\sigma_g 2\sigma_u 4\sigma_g 3\sigma_u$ (0.99)	$D_{\infty h}$ $R=6.558$	$76(\pi_u)$ $132(\sigma_g)$ $261(\sigma_u)$	1.81	1.785
$^5B_1$	$3a_1 4a_1 1b_1 5a_1$ (0.95)	C_{2v} $R=6.439$ $\angle=43.640$	$155(a_1\text{bend})$ $340(a_1)$ $100i(b_2)$	2.29	2.122
$^5A_2$[b]	$3a_1 2b_2 1b_1 5a_1$ (0.84)+ $3a_1 2b_2 4a_1 1b_1$ (0.41)	C_{2v} $R=5.276$ $\angle=111.531$	$27(a_1\text{bend})$ $273(a_1)$ $?(b_2)$	2.22	2.054
$^5\Sigma_u^-$	$3\sigma_g 2\sigma_u 1\pi_u^2$ (0.91)	$D_{\infty h}$ $R=5.289$	$56(\pi_u)$ $192(\sigma_g)$ $314(\sigma_u)$	2.21	2.126

[a]CAS SCF frequencies obtained with the active space of seven a_1, two a_2, three b_1, and five b_2 orbitals.
[b]SA CAS SCF geometry optimization; relative energies based on the $^5B_1$ results and the SA CAS SCF difference between $^5B_1$ and $^5A_2$.

differs from VDE by at least the FOJT stabilization energy ($^2E'\rightarrow{}^2B_2$). In fact, the QCI difference is 0.134 eV, whereas our stabilization energy is only 0.065 eV.

The QCI VDE for the $^4A_2'(a_1'e'^2)+e\leftarrow{}^3A_2'$ transition is 1.755 eV for Li_3^-. The resulting neutral $^4A_2'$ is the lowest energy quartet for D_{3h} geometries. The difference between this VDE and EA_a is predicted to be small since the $^4A_2'$ neutral is also geometrically stable at D_{3h} geometries with an equilibrium $M-M$ distance of 6.01 a.u.

It is worth noting that our electron detachment energies from the $^3A_2'$ state discussed above (0.761 and 1.755 eV) differ from the experimental peaks at 1.309 and 2.003 eV[8] which derive from the *linear* singlet form of Li_3^-. This makes detection of the $^3A_2'$ anion plausible, providing a significant

TABLE V. Electron vertical detachment energies (VDE) and adiabatic electron affinities (EA_a) in eV for different anionic states of Li_3^-.

Transition	Method	VDE	EA_a
$^2\Sigma_u^+ + e \leftarrow {}^1\Sigma_g^+$	CAS	1.27	1.02[a]
$^2\Sigma_u^+ + e \leftarrow {}^1\Sigma_g^+$	QCI	1.322[b]	1.005[a]
$^2\Sigma_g^+ + e \leftarrow {}^1\Sigma_g^+$	CAS	1.94	1.93
$^2\Sigma_g^+ + e \leftarrow {}^1\Sigma_g^+$	QCI	1.992[c]	1.995
$^2E' + e \leftarrow {}^3A_2'$	CAS	0.68	0.56[a]
$^2E' + e \leftarrow {}^3A_2'$	QCI	0.761	0.627[a]
$^4A_2' + e \leftarrow {}^3A_2'$	CAS	1.63	1.63
$^4A_2' + e \leftarrow {}^3A_2'$	QCI	1.755	1.759
$^4A_2' + e \leftarrow {}^5A_1''$	CAS	0.40	0.40
$^4A_2' + e \leftarrow {}^5A_1''$	QCI	0.563	0.567
$^4A_2' + e \leftarrow {}^5A_2'$	CAS	0.29	0.27
$^4A_2' + e \leftarrow {}^5A_2'$	QCI	0.465	0.438

[a]The state of the neutral is $^2B_2$ for the adiabatic transition.
[b]The experimental VDE is 1.309±0.005 eV (Ref. 8).
[c]The experimental VDE is 2.003±0.005 eV (Ref. 8).

concentration of the triplet isomer can be produced in the anionic beam.

For today, there is no experimental evidence for the $^3A_2'$ state of the alkali metal trimers. However, an unidentified excited electronic state of Cu_3^- was observed by Leopold *et al.* in photoelectron spectroscopy experiments using 2.540 and 2.707 eV photons.[30] The strong peak with VDE of 2.35–2.55 eV, assigned to a linear structure, was accompanied by a feature which is more than two orders of magnitude weaker and possesses a VDE of ~1.5 eV. It was verified that the weak feature is due neither to a copper oxide (e.g., $Cu_2O_4^-$) nor to a copper cluster containing any other foreign species.[30] Thus the authors of Ref. 30 assigned the weak band to an electronically excited state of Cu_3^-. Of course, the peaks observed for Cu_3^- have much higher VDEs than those for the alkali metal trimers, consistent with the difference in the bulk work functions. Hence, it may well be that the $^3A_2'$ state of Cu_3^- was observed by Leopold *et al.*[30]

b. $^1E'$ *state.* The state $1\ ^1E'$ is subject to FOJT distortion which lowers the molecular symmetry to C_{2v} and produces two distinct electronic states

$$1\ ^1E' \begin{cases} 1\ ^1A_1 : c_1 3a_1^2 2b_2^2 - c_2 3a_1^2 4a_1^2 \\ 1\ ^1B_2 : 3a_1^2 4a_1 2b_2 \end{cases}$$

TABLE VI. The CAS SCF electron vertical detachment energies (VDE) and adiabatic electron affinities (EA_a) in eV for different anionic states of Na_3^-.

Transition	VDE	EA_a
$^2\Sigma_u^+ + e \leftarrow {}^1\Sigma_g^+$	1.13[a]	1.05[b]
$^2\Sigma_g^+ + e \leftarrow {}^1\Sigma_g^+$	1.73[c]	1.70
$^2E' + e \leftarrow {}^3A_2'$	0.78	0.62[b]
$^4A_2' + e \leftarrow {}^3A_2'$	1.52	1.44
$^4A_2' + e \leftarrow {}^5A_1''$	0.25	0.22
$^4A_2' + e \leftarrow {}^5A_2'$	0.12	0.11

[a]The experimental VDE is 1.158±0.01 eV (Ref. 7).
[b]The state of the neutral is $^2B_2$ for the adiabatic transition.
[c]The experimental VDE is 1.813±0.01 eV (Ref. 7).

TABLE VII. Harmonic vibrational frequencies (cm^{-1}) for $^1B_2$ state of Li_3^- obtained with different CAS spaces. The full-valence CAS SCF geometry was used (R=6.193 a.u., angle=55.19°). Orbitals $1a_1$, $2a_1$, and $1b_2$ are doubly occupied in every configuration state function.

Active space	$\nu_{bending}$	$\nu_{sym.\ stretch}$	$\nu_{asym.\ stretch}$
Two a_1 one b_2	184	265	227*i*
Two a_1 one b_1 one b_2	173	256	227*i*
Three a_1 one b_1 one b_2	154	230	368*i*
Four a_1 one b_1 two b_2	179	257	242*i*
Four a_1 one a_2 two b_1 two b_2	178	256	484*i*
Four a_1 one a_2 two b_1 three b_2	178	254	328*i*
Five a_1 one a_2 two b_1 four b_2 (full valence)	175	254	427
Six a_1 one a_2 two b_1 four b_2	177	254	1033
Six a_1 two a_2 three b_1 four b_2	176	254	1571
Seven a_1 two a_2 three b_1 five b_2	173	252	658*i*

with the $1\ ^1A_1$ and $1\ ^1B_2$ states favoring obtuse and acute triangle, respectively. The coefficients c_1 and c_2 are equal in D_{3h} geometries, but not at the distorted structures.

The $1\ ^1A_1$ state correlates with the lowest energy linear $^1\Sigma_g^+$ isomer of M_3^- and no barrier was observed along this rearrangement path. As M_3^- approaches the linear structure, the role of the $3a_1^2 4a_1^2$ configuration decreases (i.e., the absolute value of the c_2 coefficient uniformly decreases).

For the $1\ ^1B_2$ offspring of the $1\ ^1E'$ state the full valence CAS SCF geometry optimization led to a stationary point with R=6.193 a.u. and an angle of 55.19°. The harmonic frequencies of all normal modes are real (see the seventh row in Table VII) which initially led us to conclude that another electronically stable minimum for M_3^- had been found.

However, when we performed additional CAS SCF calculations with active spaces smaller and larger than the full-valence space, the harmonic frequencies reported in Table VII were obtained. The frequencies for the symmetric stretching and bending modes are stable within 35 cm^{-1}. The asymmetric stretching mode frequency is imaginary for small CAS spaces, real for the full valence, and again imaginary for the largest CAS space considered. Clearly, the full-valence CAS SCF prediction as to the nature of the $^1B_2$ stationary point seems to be misleading. This is an annoying artifact of nonfull CI calculations.

The behavior of the b_2 mode frequency as a function of calculation quality must be related to symmetry breaking.[31] Previous numerical observations indicated that this may happen in single-configurational calculations in which some correlation effects could be included in the wave function at the expense of incorporating extra configurations of the wrong symmetry. A remedy against this artifact was to include in the configuration space all important configurations of the correct symmetry. Here, however, we report anomalies at the full-valence CAS SCF level which is believed to be satisfac-

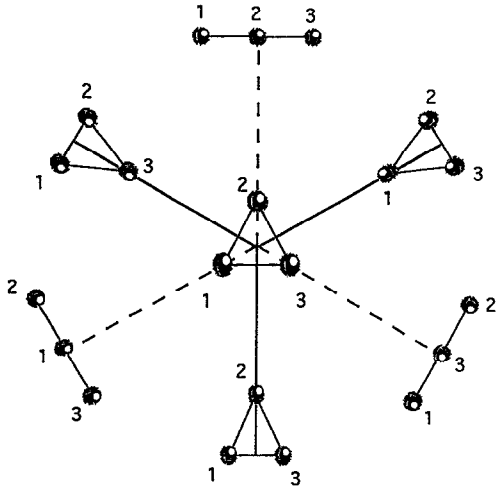

FIG. 2. The nonrigid intramolecular rearrangement for the $^1E'$ anionic state with the linear structures ($^1\Sigma_g^+$) corresponding to minima and the C_{2v} structures ($^1B_2$) to transition states. The reaction path goes through C_s geometries.

tory in chemical applications, though computationally demanding. On the other hand, the b_2 mode frequencies are consistently imaginary in small valence spaces. The reported results indicate that the anionic $^1B_2$ stationary point is actually a transition state.

The origin of the b_2 frequency instability definitely requires further investigations. Our preliminary results indicate that the full-valence CAS SCF energy is very flat with respect to the $a_1\langle$--$\rangle b_2$ orbital rotations. This may affect the stability of the solutions of the coupled-MCSCF equations for the first-order geometrical responses. The flatness of the full-valence energy is probably related to the very small number of valence electrons in the case of alkali metal clusters.

The three equivalent $^1B_2$ transition states connect three equivalent linear ground state structures of $^1\Sigma_g^+$ symmetry, with the reaction path going through C_s geometries. The graph representing this nonrigid intramolecular rearrangement is shown in Fig. 2. The initial distortion from the linear structure involves the motion along the bending (π_u) and antisymmetric stretching (σ_u) modes, whereas that from the C_{2v} structure is primarily along the antisymmetric stretching b_2 mode. The energy barrier for the rearrangement is 0.68 eV at the CAS SCF level of theory. The QCI approach is inapplicable for the $^1B_2$ state, similarly as for the $^1\Sigma_u^+$ state of the dimer.

c. $^5A_1''$ *state.* This anionic state may by characterized as the lowest energy quartet state of the neutral [i.e., $^4A_2'(2a_1'2e'^2)$] with an extra, high-spin coupled electron in the $1a_2''$ orbital whose electronic density is distributed above and below the molecular plane. Hence, it does not significantly disturb the bonding of neutral $^4A_2'$, for which the electron density is accommodated primarily in molecular plane.

Indeed, the equilibrium R for this $^5A_1''$ state (5.80 a.u.) is even smaller than that of the $^4A_2'$ neutral, which is 6.01 a.u., probably due to the constructive interaction among the np AOs in the $1a_2''$ MO. The similarity between the neutral $^4A_2'$ and the anion $^5A_1''$ manifests also in the CAS SCF harmonic frequencies which are 187 (e') and 221 (a_1') for $^5A_1''$ and 189 (e') and 218 (a_1') for $^4A_2'$.

In the nonrelativistic approximation, the $^5A_1''$ state is a genuine bound state. The VDE to the lowest neutral $^4A_2'$ state is 0.56 eV which is even lower than EA_a values for the $^2B_2 + e \leftarrow {}^3A_2'$ transition. Therefore, the $^5A_1''$ state may also be amenable to photoelectron spectroscopy detection.

d. $^5A_2'$ *state.* This state may be characterized as the neutral $^4A_2'$ with an extra high-spin coupled electron, this time in the $3a_1'$ orbital. The extra electron density is in the molecular plane, so larger differences are expected between the neutral and the anion, than those reported above for the $^5A_1''$ ion.

Indeed, despite the bonding properties of the $3a_1'$ orbital, the equilibrium internuclear distance in $^5A_2'$ is larger by 0.3 a.u. than in the neutral $^4A_2'$ and the vibrational frequencies for the $^5A_2'$ state are 130 (e') and 184 (a_1'), thus smaller than those for the $^4A_2'$ neutral.

In the nonrelativistic approximation, the $^5A_2'$ anion is another bound electronic state. The transition $^5A_2' \leftarrow {}^5A_1''$ has a vertical excitation energy of 994 cm^{-1} (QCI) or 1178 cm^{-1} (FOCI) and the oscillator strength 0.013 (FOCI). This prediction should help in future experimental search for anionic quintet states.

The extra electron is less bound in this $^5A_2'$ state than in the $^5A_1''$ state. For Li_3^- the value of the $^5A_2'$ VDE is 0.29 (CAS) and 0.47 (QCI). For Na_3^-, the VDE value of 0.12 eV (CAS) is even smaller.

The $^5A_2'$ state correlates with a higher in energy $^5\Pi_g$ linear state, as the $^5A_1''$ state does. Both $^5A_2'$ and $^5A_1''$ states may be considered as molecular analogs of the core-excited atomic anionic states studied by Bunge and collaborators.[32]

2. $D_{\infty h}$ geometries and the C_{2v} neighborhood

a. $^1\Sigma_g^+$ *state.* This is the lowest energy isomer of M_3^-. The CI wave function is dominated by the configuration $3\sigma_g^2 2\sigma_u^2$ and the $2\sigma_u$ orbital displays an antibonding interaction between the terminal Li atoms; hence the nature of the doubly occupied $2\sigma_u$ orbital helps preserve linear structure. The same effect may cause the equilibrium $M-M$ distance to be larger (by 0.24 a.u.) than in the ground state linear neutral $^2\Sigma_u^+(3\sigma_g^2 2\sigma_u)$.

The latter state, however, is geometrically unstable with respect to bending motion since the effect of the singly occupied $2\sigma_u$ orbital is apparently overweighed by the preference of the doubly occupied $3\sigma_g$ orbital for D_{3h} geometry. The $^2\Sigma_u^+$ state correlates with the $^2B_2$ state which has a minimum at $R=5.34$ a.u. and an angle of 72.63°.

The VDE of the $^2\Sigma_u^+ + e \leftarrow {}^1\Sigma_g^+$ transition is 1.322 eV and the EA_a is smaller by 0.317 eV, whereas the linearization energy for $^2B_2$ neutral is 0.289 eV. Due to significant difference between the anionic and neutral equilibrium structure, the photodetachment peak is expected to display a significant Franck–Condon width.

Another neutral state that is related to the $^1\Sigma_g^+$ anion

through a single electron process is the $^2\Sigma_g^+$ state, with the dominant configuration $3\sigma_g 2\sigma_u^2$. This electronic configuration suggests a linear equilibrium structure and a bond length even longer than in the $^1\Sigma_g^+$ anion. This is indeed the case as the equilibrium R for $^2\Sigma_g^+$ is 5.96 a.u.

The photodetachment peak related to the $^2\Sigma_g^+ + e \leftarrow {}^1\Sigma_g^+$ transition has a VDE of 1.992 eV. Since there is small relaxation in the neutral equilibrium geometry, the EA_a of 1.995 eV is quite similar to VDE, so the peak is expected to be sharp.

Our theoretical results are in a good agreement with the experimental data which predict VDEs of 1.309 ± 0.005 eV (wide peak) and 2.003 ± 0.005 eV (sharp peak) for transitions leading to $^2\Sigma_u^+$ and $^2\Sigma_g^+$ products, respectively.[8]

b. $^3\Sigma_u^+$ *state.* The dominant configuration of this state is $3\sigma_g^2 2\sigma_u 4\sigma_g$ which correlates with the D_{3h} $^3A_2'$ state. Since the orbital energies of $2\sigma_u$ and $4\sigma_g$ have opposite dependence on bending angle, the surface of the $^3\Sigma_u^+$ state is expected to be quite flat with respect to bending. In fact, our bending frequencies are only 53 cm^{-1} at both the CAS SCF and MP2 levels. Since they are real, a transition state is anticipated when a $D_{\infty h}$ structure is approached from the D_{3h} minimum. We actually performed a transition state search and found one at an angle of 142° and $R=5.95$ a.u., with an energy higher by 0.271 eV (CAS) than at the D_{3h} minimum, and an imaginary frequency of 34 cm^{-1}. This transition state was, however, 0.002 eV *lower* than the linear $^3\Sigma_u^+$ minimum. Approaching the linear structure, another C_{2v} minimum was found at $R=5.99$ a.u. and an angle of 169° with an energy only 0.002 eV below the transition state and a real bending frequency of 23 cm^{-1}. We abandoned looking for other transition states since the energy changes involved are below the accuracy of our CAS SCF approach. The most reasonable conclusion to draw is that the surface is actually very flat with respect to the bending motion. Interestingly, the optimal distance R remains within the range of 5.9–6.0 a.u. for all the stationary points found.

The $^3\Sigma_u^+$ state is electronically stable for linear geometries, and the value of EA_a for the transition leading to the lowest energy $^2\Sigma_u^+$ neutral is still 0.589 eV. We thus conclude that the lowest triplet anionic state is electronically stable for D_{3h}, C_{2v}, and $D_{\infty h}$ geometries.

c. $^5\Pi_g$ *state.* The dominant configuration of this state is $3\sigma_g 2\sigma_u 4\sigma_g 1\pi_u$. Despite simple molecular orbital arguments, see Fig. 1, and the fact that this state correlates with the two lowest D_{3h} $^5A_1''$ and $^5A_2'$ states, the $^5\Pi_g$ state lies above the $^5\Sigma_g^+(3\sigma_g 2\sigma_u 4\sigma_g 3\sigma_u)$ state by 0.117 eV. The lower $^5\Sigma_g^+$ state, which is electronically stable only in the neighborhood of the linear structure, will be discussed in Sec. IV B.

The CAS SCF frequencies for the $^5\Pi_g$ state indicate that the Renner–Teller splitting for the bending modes is less than 0.5 cm^{-1}. The fact that both such frequencies are real indicates that the $^5A_1''(^5A_2)$ and $^5A_2'(^5B_2)$ states correlate to the $^5\Pi_g$ state through transition states. Our searches for these transition states started at D_{3h} geometries and moved uphill along the bending mode. Stationary points at $R=6.02$ a.u., angle 126.8°, $\nu_{bend}=57i$ cm^{-1}, and $R=6.07$ a.u., angle 131.4°, $\nu_{bend}=47i$ cm^{-1} were found for the $^5A_2$ and $^5B_2$ states, respectively. The energies of these transition states are 0.02 eV below ($^5A_2$) and 0.01 eV above ($^5B_2$) the energy of the $^5\Pi_g$ minimum. Clearly, the surfaces become very flat from the angle of ~120°; for this reason we did not pursue further study for C_{2v} geometries closer to the linear structure since the accuracy of our CAS SCF data would not be sufficient. The flatness of the $^5A_2$ and $^5B_2$ surfaces is probably related to the opposite angular dependence of the $2b_2$ and $4a_1$ orbital energies, see Fig. 1.

The fact that the $^5\Sigma_g^+$ state is lower than the $^5\Pi_g$ state at linear geometries indicates that, in a C_{2v} geometry, there is a crossing between the $^5A_1(^5\Sigma_g^+)$ and the $^5B_2$ component of the $^5\Pi_g$ state. In this region, the $^5B_2$ state becomes geometrically unstable with respect to the b_2 vibrational mode due to second-order Jahn–Teller coupling.[33] In addition, "hopping" to the $^5A_1(^5\Sigma_g^+)$ surface can take place. Both factors will decrease the lifetime of the $^5A_2'$ state, in addition to the radiative decay channel.

The electronic stability of the $^5\Pi_g$ state has to be considered with respect to two low-energy neutral quartet states, $^4\Sigma_u^+(3\sigma_g 2\sigma_u 4\sigma_g)$ and $^4\Pi_g(3\sigma_g 2\sigma_u 1\pi_u)$. The equilibrium geometries of the former ($R=7.47$ a.u.) and the latter ($R=5.41$ a.u.) differ significantly from the equilibrium R of $^5\Pi_g$, which is 6.08 a.u. Hence, a major difference is expected between the corresponding VDE and EA_a energies: VDE = 0.656 and 0.783 eV, $EA_a=0.603$ and 0.640 eV for the $^4\Sigma_u^+$ and $^4\Pi_g$ transitions, respectively.

We conclude that the $^5A_1''$ and $^5A_2'$ quintet anionic states are electronically stable in D_{3h}, C_{2v}, and $D_{\infty h}$ geometries.

B. Locally electronically stable species

1. $1\,^1A_1'$ state

This state results from the same $2a_1'^2 2e'^2$ configuration that produces the $^1E'$ and $^3A_2'$ states. Even though this state is not subject to FOJT distortion, we write its approximate CI wave function $c_1 3a_1^2 2b_2^2 + c_2 3a_1^2 4a_1^2$ in the C_{2v} orbital symmetry notation to make the difference between $1\,^1E'$ and $1\,^1A_1'$ transparent.

The geometry of this state was optimized within D_{3h} symmetry and the geometrical Hessian analysis indicates that this is a minimum structure indeed, see Table IV. The anion is electronically stable with respect to the lowest $^2E'(2a_1'^2 2e')$ state of the neutral by 0.065 eV (CAS level).

Recall that the $^2E'$ state of the neutral is FOJT unstable and we found that the $^2B_2$ minimum of Li_3 is lower by 0.058 eV (CAS) than the D_{3h} $^1A_1'$ minimum of Li_3^-. Clearly, the anionic and neutral surfaces must cross in C_{2v} symmetry not far from the D_{3h} manifold. The electronic stability of the anion is thus restricted to a small part of the potential energy surface so this state cannot be long lived.

2. $^3\Sigma_g^+$ state

This is a state with two important configurations: $3\sigma_g 2\sigma_u^2 4\sigma_g$ and $3\sigma_g^2 2\sigma_u 3\sigma_u$. Its minimum energy geometry was found at $R=6.04$ a.u. where the bending mode frequency is only 86 cm^{-1}. Hence, C_{2v} geometries are easily accessible. This state correlates at D_{3h} geometries to an electronically unstable $^3E'$ state. Therefore, the electronic stabil-

ity is restricted to linear geometries and their close neighborhood; at linear geometry, the state is electronically stable with respect to the lowest neutral $^2\Sigma_u^+$ state by 0.340 eV (EA_a).

3. $^3\Pi_g$ state

For this anionic state, the dominant configuration is $3\sigma_g^2 2\sigma_u 3\pi_u$. A geometry minimum was found at $R=5.53$ a.u. with a Renner–Teller splitting of 7 cm^{-1}. The bending frequencies are low, hence C_{2v} geometries are easily accessible. The $^3B_2$ component of this $^3\Pi_g$ state correlates with the same D_{3h} $^3E'$ state as the $^3\Sigma_g^+$ state does. The $^3A_2$ component of this state correlates with an electronically unstable $^3E''$ state. Therefore, the electronic stability of the $^3\Pi_g$ state is restricted to linear geometries and their close neighborhood where it is stable with respect to the lowest neutral $^2\Sigma_u^+$ state by 0.173 eV (EA_a).

4. $^5\Sigma_g^+$ state

This is the lowest energy quintet state at linear geometries and has a dominant configuration $3\sigma_g 2\sigma_u 4\sigma_g 3\sigma_u$. Due to the counterbalancing energy dependence of the $2\sigma_u$ and $4\sigma_g$ orbitals, the surface is expected to be flat with respect to bending. In fact, the bending frequency is only 76 cm^{-1} and C_{2v} geometries are easily accessible.

In D_{3h} symmetry, this state correlates with the $^5E'(2a_1'2e'^2 3e')$ state which is electronically unstable. Hence, the electronic stability of the $^5\Sigma_g^+$ state is restricted to linear geometries and their close neighborhood, where a crossing with the $^5B_2$ $^5B_2(^5A_2')$ state takes place, accompanied by second-order Jahn–Teller instability and possibility of surface "hopping."

At linear geometries, the $^5\Sigma_g^+$ state is electronically stable with respect to the two lowest quartet states of the neutral: VDE=0.726 and 1.073 eV, EA_a=0.720 and 0.756 eV, for the $^4\Sigma_u^+$ and $^4\Pi_g$ state, respectively.

5. $^5E''$ state

The $^5E''$ state is a candidate for a long-lived, metastable, pseudorotating state. The electronic stability of this state is discussed below, for different regions of the potential energy surface.

In D_{3h} geometries, the $^5E''(2a_1'2e'1a_2''3a_1')$ state is electronically unstable with respect to the ground quartet $^4A_2'(2a_1'2e'^2)$ state. However, since the $2a_1'2e'1a_2''3a_1'$ configuration differs from the $2a_1'2e'^2ke''$ configuration needed to produce the $^4A_2'$ neutral (ke'' denotes an e'' symmetry orbital for the outgoing electron) by two spin–orbital occupancies, the coupling to this detachment channel is expected to be weak. Among configurations which contribute to $^5E''$ and simultaneously can couple to the $^4A_2'$ neutral in a one-electron process, the largest CI coefficient (only 0.12) was found for the $2a_1'2e'^21e''$ configuration. The neutral state $^4E''(2a_1'2e'1a_2'')$, to which the anion could couple in a one-electron process, is higher in energy than the anion by 0.23 eV (CAS level at the cation equilibrium geometry).

The $^5E''$ state is FOJT unstable, producing $2\,^5A_2$ and $1\,^5B_1$ states which favor obtuse and acute structures, respectively, consistent with the bending angular dependence of the $4a_1$ and $2b_2$ orbitals. A stationary point on the $^5B_1(3a_1 4a_1 1b_1 5a_1)$ surface, with $R=6.44$ a.u. and an angle of 43.6°, proved to be a transition state, with a negative curvature along the asymmetric stretching mode, see Table IV. At this geometry, the energy of the $^5B_1$ state is lower than the energy of the lowest quartet $^4B_2$ neutral state by 0.04 eV (CAS) and 0.22 eV (QCI). Hence, the electronic instability of the anionic quintet state is probably restricted to D_{3h} geometries and the close neighborhood.

Geometry optimization for the $2\,^5A_2$ offspring of the $^5E''$ state was performed in the state-averaged CAS SCF procedure, to avoid "root flipping."[34] Three electronic states were state averaged with equal weighting factors: $1\,^5A_2(^5A_1'')$, $1\,^5B_2(^5A_2')$, and $2\,^5A_2(^5E'')$, and the CI mixing was significant between two $^5A_2$ $3a_1 2b_2 4a_1 1b_1$ and $3a_1 2b_2 1b_1 5a_1$ configurations.

A stationary point for the $2\,^5A_2$ state was found at $R=5.28$ a.u., and an angle of 111.5°. We expect it is a minimum, but the finite difference Hessian formed in the SA CAS SCF C_{2v} optimization does not allow us to determine the b_2 mode frequency. Interestingly, at this stationary point, the energy of the lowest $^4B_2$ neutral state calculated without the SA constraint is higher by 0.14 eV than the energy of the SA optimized $2\,^5A_2$ anion. This indicates that the $2\,^5A_2$ state is electronically stable at the stationary point.

Determination of the pseudorotation barrier on the $^5E''$ surface requires a consistent calculation of the $1\,^5B_1$ and $2\,^5A_2$ energies. Hence, we recalculated the energy of $1\,^5B_1$ at its stationary point using the SA procedure involving $1\,^5A_2$, $1\,^5B_2$, and $1\,^5B_1$ states. The resulting energy was only 0.07 eV higher than the single-state CAS SCF energy and the pseudorotation barrier is estimated to be 544 cm^{-1}.

The $2\,^5A_2$ state correlates with the linear $^5\Sigma_u^-(3\sigma_g 2\sigma_u 1\pi_u^2)$ state. This is the third electronically stable anionic quintet state at the linear geometry, and is higher in energy than the $^5\Sigma_g^+$ and $^5\Pi_g$ states by 0.341 and 0.225 eV (QCI), respectively. A stationary point was found for the $^5\Sigma_u^-$ state at $R=5.29$ a.u., with a bending frequency of only 56 cm^{-1}. The anion is electronically stable with respect to the two lowest quartet states of the neutral: VDE=0.678 and 0.410 eV, EA_a=0.379 and 0.415 eV, for $^4\Sigma_u^+$ and $^4\Pi_g$, respectively.

V. SUMMARY

The alkali metal trimer anions possess more than one electronically and geometrically bound state. In addition to the known $^1\Sigma_g^+$ state, one triplet $^3A_2'$ and two quintet $^5A_1''$, $^5A_2'$ states are predicted to be electronically stable for a wide variety of geometries. The multitude of electronically bound states is probably related to the small energy separation between valence ns and np atomic orbitals in alkali metal atoms.

The linear $^1\Sigma_g^+(3\sigma_g^2 2\sigma_u^2)$ state is the lowest energy isomer of Li_3^-. Our VDE for the $^2\Sigma_u^+ + e \leftarrow {}^1\Sigma_g^+$ and $^2\Sigma_g^+ + e \leftarrow {}^1\Sigma_g^+$ transitions are 1.322 and 1.995 eV, respectively, in good agreement with the experimentally observed peaks at 1.309 ± 0.005 and 2.003 ± 0.005 eV.[8] The barrier for

nonrigid intramolecular rearrangement of the linear isomer was found to be 0.68 eV and to pass through a C_{2v} symmetry $^1B_2$ transition state.

The $^3A_2'(a_1'^2e'^2)$ anion is the lowest energy isomer in D_{3h} geometries. This triplet state remains electronically stable in C_{2v} and $D_{\infty h}$ geometries. Our VDE for the $^2E' + e \leftarrow {}^3A_2'$ and $^4A_2' + e \leftarrow {}^3A_2'$ transitions in Li_3^- are 0.761 and 1.755 eV, respectively. Hence, the peaks should be clearly distinct from the transitions involving the linear $^1\Sigma_g^+$ anion, thereby suggesting further experimental study.

After this work was completed, we were pleased to find that Bauschlicher *et al.*[35] also invoked the $^3A_2'$ anionic state to explain the weak feature in the photoelectron spectrum of Cu_3^-[30] and found a VDE for the triplet D_{3h} isomer of Cu_3^-, calculated at the modified coupled pair functional level of theory, in good agreement with the experimental finding. Interestingly, the weak feature ascribed to the $^3A_2'$ anion was not observed in the later work from the Lineberger group,[36] presumably due to cooler ion source conditions.

Two quintet $^5A_1''$ and $^5A_2'$ anionic states were also identified that may be thought of as the lowest energy quartet $^4A_2'(a_1'e'^2)$ state of the neutral with an extra high-spin coupled electron attached to a a_2'' or a_1' orbital, respectively. These quintet states are genuine bound states in the nonrelativistic approximation, and may be considered as molecular analogs of core-excited atomic anionic states studied earlier.[32] The vertical excitation energy for the radiative $^5A_2' \leftarrow {}^5A_1''$ transition is ~ 1000 cm^{-1} and the oscillator strength is 0.013.

For the $^5A_1''$ and $^5A_2'$ states of Li_3^-, the vertical detachment energies to the $^4A_2'$ state neutral are 0.563 and 0.465 eV, respectively. Both quintet states remain electronically stable with respect to the lowest neutral quartet state along a bending motion path to the linear structure, where they correlate with a $^5\Pi_g$ state. When proceeding to the linear structure, the $^5A_2'(^5B_2)$ state intersects with the $^5\Sigma_g^+(^5A_1)$ state, so geometrical instability must develop along the b_2 mode and surface hopping may take place.

The lithium trimer also possesses many anionic states which are electronically stable for restricted geometries only. The most interesting of them is probably the pseudorotating $^5E''$ state. It is electronically unstable in D_{3h} geometries, but stable at the stationary points of the $^5B_1$ (transition state) and $^5A_2$ (minimum) surfaces. Moreover, the $^5E''$ wave function displays properties required to be classified as a Feshbach resonance state at D_{3h} geometries.

An extension of our present conclusions to other alkali metal trimers would be important. It is encouraging that our preliminary CAS SCF results for Na_3^- are qualitatively the same as those for Li_3^-. The presence of alkali metal atoms in heteroatomic radicals may enhance an ability to form more than one electronically bound anionic state. Indeed, the whole family of lithium substituted double-Rydberg anions accommodates an excited triplet state in addition to the ground fully symmetric singlet state.[37]

ACKNOWLEDGMENTS

This work was supported by the Office of Naval Research and National Science Foundation Grant No. CHE 9116286. Computer resources of the Utah Supercomputing Institute are also gratefully acknowledged.

[1] V. Bonacic-Koutecky, P. Fantucci, and J. Koutecky, Chem. Rev. **91**, 1035 (1991).
[2] (a) J. Simons and M. Gutowski, Chem. Rev. **91**, 669 (1991); (b) M. Gutowski, J. Simons, R. Hernandez, and H. L. Taylor, J. Phys. Chem. **92**, 6179 (1988); (c) M. Gutowski and J. Simons, J. Chem. Phys. **93**, 3874 (1990); (d) **93**, 2546 (1990); (e) J. V. Ortiz, *ibid.* **87**, 3557 (1987); (f) *ibid.* **91**, 7024 (1989); (g) J. Phys. Chem. **94**, 4762 (1990).
[3] A. I. Boldyrev and J. Simons, J. Phys. Chem. **96**, 8840 (1992); **97**, 1470 (1993).
[4] M. Gutowski and J. Simons, J. Chem. Phys. (in preparation).
[5] J.-P. Wolf, G. Delacretaz, and L. Woste, Phys. Rev. Lett. **63**, 1946 (1989).
[6] Ph. Dugourd, J. Chevaleyre, M. Broyer, J. P. Wolf, and L. Woste, Chem. Phys. Lett. **175**, 555 (1990).
[7] K. M. McHugh, J. G. Eaton, G. H. Lee, H. W. Sarkas, L. H. Kidder, J. T. Snodgrass, M. R. Manaa, and K. H. Bowen, J. Chem. Phys. **91**, 3792 (1989); K. H. Bowen and J. G. Eaton, in *The Structure of Small Molecules and Clusters*, edited by R. Naaman and Z. Vager (Plenum, New York, 1988).
[8] H. W. Sarkas, S. T. Arnold, J. H. Hendricks, and K. H. Bowen (unpublished).
[9] J. Blanc, M. Broyer, J. Chevaleyre, Ph. Dugourd, H. Kuhling, P. Labastie, M. Ulbricht, J. P. Wolf, and L. Woste, Z. Phys. D **19**, 7 (1991).
[10] I. Boustani and J. Koutecky, J. Chem. Phys. **88**, 5657 (1988).
[11] J. V. Ortiz, J. Chem. Phys. **89**, 6353 (1988).
[12] V. Bonacic-Koutecky, P. Fantucci, and J. Koutecky, J. Chem. Phys. **91**, 3794 (1989); **93**, 3802 (1990).
[13] H. W. Sarkas, S. T. Arnold, J. H. Hendricks, and K. H. Bowen, Z. Phys. D (submitted).
[14] J. A. Pople, M. Head-Gordon, and K. Raghavaachari, J. Chem. Phys. **87**, 5968 (1987).
[15] T. Dunning (unpublished results).
[16] T. Clark, J. Chandrasekhar, G. Spitznagel, and P. van Rague Schleyer, J. Comput. Chem. **4**, 294 (1982).
[17] J. S. Binkley and J. A. Pople, J. Chem. Phys. **66**, 879 (1977).
[18] A. D. McLean and G. S. Chandler, J. Chem. Phys. **72**, 5639 (1980).
[19] M. J. Frish, J. A. Pople, and J. S. Binkley, J. Chem. Phys. **80**, 3265 (1984).
[20] M. M. Francl, W. J. Pietro, W. J. Hehre, J. S. Binkley, M. S. Gordon, D. J. DeFrees, and J. A. Pople, J. Chem. Phys. **77**, 3654 (1982).
[21] W. Muller and W. Meyer, J. Chem. Phys. **80**, 3311 (1984); W. Muller, J. Flesch, and W. Meyer, *ibid.* **80**, 3297 (1984).
[22] The Utah MESS-KIT is a suite of highly modular codes that were programmed in-house to give a variety of electronic structure functionalities by J. A. Nichols, M. R. Hoffmann, R. A. Kendall, H. L. Taylor, D. W. O'Neal, E. Earl, R. Hernandez, M. Gutowski, J. Boatz, K. Bak, J. Anchell, X. Wang, M. Feyereisen, and J. Simons.
[23] J. Nichols, H. Taylor, P. Schmidt, and J. Simons, J. Chem. Phys. **92**, 340 (1990); J. Simons, P. Jørgensen, H. Taylor, and J. Ozment, J. Phys. Chem. **87**, 2745 (1983); D. O'Neal, H. Taylor, and J. Simons, *ibid.* **88**, 1510 (1984); A. Banerjee, N. Adams, J. Simons, and R. Shepard, *ibid.* **89**, 52 (1985); H. Taylor and J. Simons, *ibid.* **89**, 684 (1985); C. J. Cerjan and W. H. Miller, J. Chem. Phys. **75**, 2800 (1981); J. Baker, J. Comp. Chem. **9**, 465 (1988); J. Baker, *ibid.* **7**, 385 (1986).
[24] K. K. Docken and J. Hinze, J. Chem. Phys. **57**, 4928 (1972).
[25] K. L. Bak, J. Boatz, and J. Simons, Int. J. Quantum. Chem. **40**, 361 (1991); K. L. Bak and J. Simons, Theor. Chim. Acta **82**, 7 (1992).
[26] Revision A, M. J. Frisch, G. W. Trucks, M. Head-Gordon, P. M. Gill, M. W. Wong, J. B. Foresman, B. G. Johnson, H. B. Schlegel, M. A. Robb, E. S. Replogle, R. Gomperts, J. L. Andres, K. Raghavachari, J. S. Binkley, C. Gonzales, R. L. Martin, D. J. Fox, D. J. DeFrees, J. Baker, J. J. P. Stewart, and J. A. Pople (Gaussian Inc., Pittsburgh, PA, 1990).
[27] (a) M. Dupuis, D. Spangler, and J. J. Wendolowski, National Resource for Computations in Chemistry Software Catalog, University of California: Berkeley, CA, 1980, Program QG01; (b) M. W. Schmidt, K. K. Baldridge, J. A. Boatz, J. H. Jensen, S. Koseki, M. S. Gordon, K. A. Nguyen, T. L. Windus, and S. T. Elbert, QCPE Bull. **10**, 52 (1990).

[28] C. E. Moore, *Atomic Energy Levels* (National Bureau of Standards, Washington, DC, 1949).
[29] H. Hotop and W. C. Lineberger, J. Phys. Chem. Ref. Data **14**, 731 (1985).
[30] D. G. Leopold, J. Ho, and W. C. Lineberger, J. Chem. Phys. **86**, 1715 (1987).
[31] W. D. Allen, D. A. Horner, R. L. Dekock, and R. B. Remington, Mol. Phys. **133**, 11 (1989); J. H. van Lenthe and F. B. van Duijneveldt, J. Chem. Phys. **81**, 3168 (1984); E. R. Davidson and W. T. Borden, J. Phys. Chem. **87**, 4783 (1983).
[32] (a) A. V. Bunge and C. F. Bunge, in *Computational Chemistry, Structure, Interactions, and Reactivity*, edited by S. Fraga (Elsevier, Amsterdam, 1992), p. 355; (b) C. F. Bunge, Phys. Rev. A **22**, 1 (1980); (c) C. F. Bunge, Nucl. Instrum. Methods **202**, 299 (1982).
[33] J. Simons, *Energetic Principles of Chemical Reactions* (Jones and Bartlett, Portola Valley, CA, 1983).
[34] J. Olsen, P. Jorgensen, and D. L. Yeager, J. Chem. Phys. **76**, 527 (1982).
[35] J. C. W. Bauschlicher, Jr., S. R. Langhoff, and P. R. Taylor, J. Chem. Phys. **88**, 1041 (1988).
[36] J. Ho, K. M. Ervin, and W. C. Lineberger, J. Chem. Phys. **93**, 6897 (1990).
[37] M. Gutowski and J. Simons, J. Chem. Phys. **100**, 1308 (1994); M. Gutowski and J. Simons, J. Phys. Chem. (to be published).
[38] K. P. Huber and G. Herzberg, *Molecular Spectra and Molecular Structure* (Van Nostrand Reinhold, New York, 1979), Vol. 4.
[39] V. Bonacic-Koutecky, P. Fantucci, and J. Koutecky, Chem. Phys. Lett. **166**, 32 (1990).
[40] D. D. Konowalow, M. E. Rosenkrantz, and M. L. Olson, J. Chem. Phys. **72**, 2612 (1980).
[41] M. L. Olson and D. D. Konowalow, Chem. Phys. **21**, 393 (1977).
[42] V. Bonacic-Koutecky, P. Fantucci, and J. Koutecky, Chem. Phys. Lett. **146**, 518 (1988).